Optical investigation of three-dimensional human skin equivalents: A pilot study

Akhil Kallepalli*[1] | Blake McCall[2] | David B James[1] | Sarah Junaid[2] | James Halls[3] | Mark A Richardson[1]

[1]Sensors Group, Centre for Electronic Warfare, Information and Cyber, Cranfield University, Defence Academy of the UK, Shrivenham, United Kingdom SN6 8LA
[2]Aston Institute of Materials Research, Engineering and Applied Sciences, Aston University, United Kingdom B4 7ET
[3]Department of Radiology, The Great Western Hospital, Marlborough Road, Swindon, United Kingdom SN3 6BB

Correspondence
*Akhil Kallepalli, Email: a.kallepalli@cranfield.ac.uk

Present Address
Defence Academy of the UK, Shrivenham Swindon SN6 8LA

Human skin equivalents (HSEs) are three-dimensional living models of human skin that are prepared *in vitro* by seeding cells onto an appropriate scaffold. They recreate the structure and biological behaviour of real skin, allowing the investigation of processes such as keratinocyte differentiation and interactions between the dermal and epidermal layers. However, for wider applications, their optical and mechanical properties should also replicate those of real skin. We therefore conducted a pilot study to investigate the optical properties of HSEs. We compared Monte Carlo simulations of (1) real human skin and (2) two-layer optical models of HSEs with (3) experimental measurements of transmittance through HSE samples. The skin layers were described using a hybrid collection of optical attenuation coefficients. A linear relationship was observed between the simulations and experiments. For samples thinner than 0.5 mm, an exponential increase in detected power was observed due to fewer instances of absorption and scattering.

KEYWORDS:
tissue engineering, lasers, TracePro, Monte Carlo

1 | INTRODUCTION

A human skin equivalent (HSE) or organotypic culture is a three-dimensional (3D) living model replicating the biological properties and interactions of human skin. HSEs were developed to provide tissue models with characteristics similar to skin *in vivo*, allowing the investigation of structural and functional interactions. Although two-dimensional (2D) histological samples allow the identification of cells and the *post hoc* analysis of their interactions, it is not possible to follow interactions between cells in real time. Also, the *ex vivo* dehydration and handling of the excised tissue changes its condition. In contrast, HSEs can

[0]**Abbreviations:** HSE, human skin equivalent; KM, Kubelka Munk theory; MC, Monte Carlo; MCML, Monte Carlo for multi-layered tissue; NHDF, normal human dermal fibroblasts; NHEK, normal human epidermal keratinocytes; RCF, relative centrifugal force; RTE, radiative transfer equation; TERT, telomerase reverse transcriptase.

be used to study the morphology, stratification, linkage and growth of human epidermis, and its interactions with the dermis during growth and development [1,2].

Mechanical and optical properties of HSEs must be comparable to skin *in vivo* for HSEs to be adopted as standards for commercial purposes (e.g. testing cosmetics) [3] and medical applications (e.g. drug testing, infection monitoring, wound healing, surgical procedures) [4]. Here, we present a pilot study to investigate the optical properties of HSEs compared to human skin. Although previous studies have used inverse models and integrating spheres to accurately characterise the properties of tissue [5–7], we focussed our study towards developing a rapid and inexpensive method supported by Monte Carlo (MC) simulations of the interactions between photons and the two-layered skin models. The two layers were modelled as semi-infinite slabs with the optical properties of the epidermis and dermis (Figure 1). The remainder of the article is organised as follows:

- Section 2 describes relevant previous research on HSEs, the optical properties of tissues, and MC methods.
- Section 3 describes the procedure we used to generate HSEs.
- Section 4 summarises the optical properties of skin from multiple studies and a hybrid set of optical quantities is used to describe the properties of the epidermis and the dermis. Subsequent MC simulations are implemented in TracePro.
- Section 5 sets out the experimental setup to measure transmittance through the HSEs.
- Sections 6 and 7 present our results, discuss the contributions of this investigation to the field, and set out our conclusions.

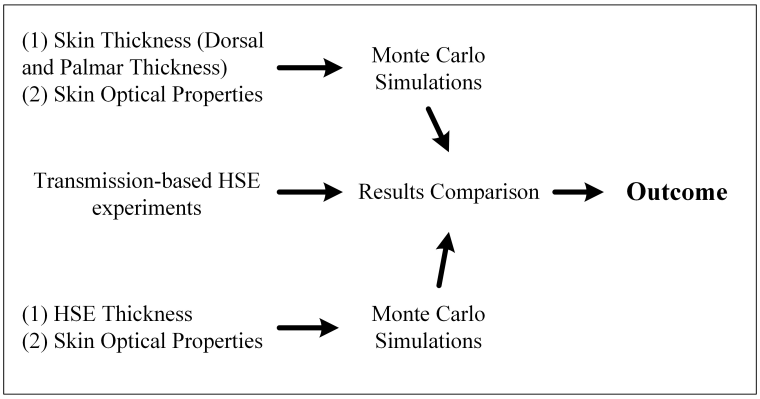

FIGURE 1 The pilot study compares Monte Carlo simulations of skin models with experimental measurements of transmittance through human skin equivalents.

2 | RELATED WORK

Engineered tissues [8] and HSEs [9,10] have been widely reviewed and the principles of light transmission have also been covered in articles [6,11–13] and textbooks [14–16]. Human skin (Fig. 2) comprises a cellular, avascular epidermis with an underlying vascular

dermis [17]. The epidermis is made up of proliferating keratinocytes that are generated in the basal layer (*stratum basale*) above the dermis, which move toward the air-skin boundary by differentiating into “prickle-like” cells (*stratum spinosum*), granular cells that lack nuclei (*stratum granulosum*) and finally the translucent cells of the stratum corneum, in a process that takes 28 days [18,19]. The epidermis and its constituents provide an environmental barrier (keratin), protection from UV radiation (melanin), immunological protection (Langerhans cells) and sensory functions (Merkel cells) [20]. The thicker underlying dermis provides mechanical support and resistance to physical shocks due to the large quantities of collagen secreted by fibroblasts [21]. The dermis also hosts sweat glands that facilitate thermo-regulation and the nerves that detect various stimuli. This layer is also responsible for the delivery of nutrients to the skin via the circulatory system [19,20,22]. The dermo-epidermal boundary is composed mainly of collagen anchoring filaments, and such filaments are also needed to maintain linkage between the layers in a HSE model [1,19].

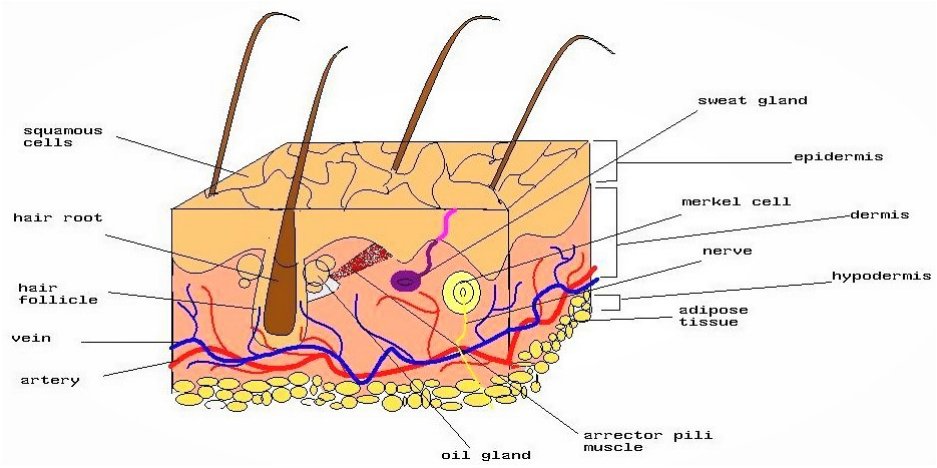

FIGURE 2 The human skin is comprised of three layers, the epidermis, dermis and hypodermis. Of the three layers, the epidermis and the dermis layers are synthesised and studied in this study. (made available under GNU Free Documentation License (GFDL))

2.1 | Human Skin Equivalents

Laboratory synthesis of HSEs begins with the construction of an acellular collagen matrix to support the cultured skin cells. Dermal fibroblasts and keratinocytes are then added to establish the dermis and epidermis, respectively. Their proliferation and consolidation into two layers then yields a 3D model of human skin. The protocol for the construction of HSEs was initially presented as a means to investigate the proliferation of skin cancer [2].

In the synthesis of tissues *in vitro*, the micro-environment of HSEs involving the basement membrane and fibroblast growth medium are key factors [1]. This directly affects the integrity of the tissue, the adhesion between layers, the proliferation and

migration of keratinocytes, and the supply of adequate nutrients to the cells [1]. By selectively removing the basement membrane and/or growth medium, the basement membrane was shown to provide indispensable support for the full-scale model and the absence of the medium delayed the model's development [1]. In the absence of both, the model did not survive beyond 9 days, highlighting the importance of fibroblasts in the growth process of the model.

Earlier studies of *in vitro* skin equivalents for grafting considered the importance of epidermal renewal for wound healing in mice [23]. Another study investigated the dermal uptake of brominated fire retardants used in fabrics by comparing dermal absorption in two commercially available HSEs [24].

Ethical and technical difficulties hinder studies related to wound healing and burn responses in the skin of living animals. There are also innate uncertainties (due to inter-species physiological and anatomical differences like skin thickness, composition of inter-cellular lipids, skin barrier function and distribution of hair follicles) when extrapolating data from animal skin to human skin [24–26]. This can be avoided using HSEs, which can accurately model processes such as the absorption of pharmaceuticals by different skin layers [9], the colonisation of skin by bacteria in hospitals [27], and resistance to percutaneous worm invasions [26]. These studies also provided detailed preparation protocols for HSEs for applications in toxicity testing, tumour modelling, infection monitoring, and wound healing [4].

More recently, HSEs have been prepared using telomerase reverse transcriptase (TERT)-immortalised keratinocytes to address the variability and limited availability of primary cells, which are extracted from juvenile foreskin or adult skin. These HSEs have been used to test recovery rates following burn and cold injuries [3]. The results were compared with HSEs derived from primary cells and *ex vivo* skin cultures. The results were promising, although additional models such as fibrin-based skin equivalents [28] should be investigated before establishing immortalised keratinocytes as a standard procedure. Accordingly, the protocol established by Carlson and colleagues [2] can be considered as the current standard as this includes considerations of the microenvironment and allows growth of tissue in a variety of extracellular matrix substrates, amongst other advantages. This protocol was adopted for construction of HSE samples for our investigation.

2.2 | Light-Tissue Interactions

The effect of the human epidermis and dermis on the transmission of light depends on the interaction between various wavelengths of incident light and resident chromophores. In addition to the refractive index and thickness of each tissue layer contributing to the interactions with light, the variations of refractive indices within the layers also impact the degree of scattering as a function of scattering cross-section and number of scatterers.

All photo-biologic interactions are governed by the wavelength of incident light, the intensity and time of exposure [16]. In the spectral region of interest, the window is limited in the UV region due to absorption by the epidermal melanosomes, and in the NIR radiation (> 1020 nm) by water. Within this window, tissues react differently to visible light, depending on their

constituents, distribution and physical properties, resulting in a mixture of reflection, absorption, scattering and transmission. Reflection occurs at the interfaces between layers [29]. The amount of light absorbed is governed by the concentration of the constituents of each tissue [13] and the scattering albedo (ratio of absorption to scattering coefficients). Photons undergo multiple reflection and scattering events before they are either absorbed by or transmitted out of the tissue model's boundaries.

In the epidermis, urocanic acid (an intermediate in histidine metabolism) and melanisation are important factors that affect attenuation at wavelengths < 300 nm [29]. At higher wavelengths, light in the epidermis is influenced by melanin alone. For normally incident light, between 4% and 7% of incident light is backscattered as regular reflectance (not specular, because the epidermal surface is not smooth and planar) for all skin types. The remaining 93-96% interacts with the tissue and result in photon scattering, transmission and/or absorption to varying degrees. Absorption by melanin is variable because it depends on concentration, distribution and the thickness of the layers. In the near-infrared region (longer wavelengths), the backscatter from the epidermis is weak (compared to scattering) and the forward scattering mainly involves off-axis refraction and large-particle scattering [29,30]. In the turbid dermis layer, the primary chromophore is haemoglobin and the dominant form of attenuation is scattering. The scattering coefficient is also inversely proportional to the wavelength, and longer wavelengths thus travel deeper into the dermis with less scattering. Greater transmittance of NIR wavelengths through the dermis and arterial blood allows pulse oximetry and oxygen saturation measurements [31].

The quantification of optical radiation and its interactions with turbid media are governed by radiative transport [32]. However, the radiative transfer equation (RTE) is difficult to solve, so approximations such as the diffusion theory are used, providing results which are computationally efficient. The diffusion approximation was used to quantify transmittance under semi-infinite boundary conditions, allowing the measurement of tissue oxygen saturation in neonates [33] and the optical absorbance of whole blood [34]. However, certain key assumptions for this theory like nearly isotropic radiance and temporal broadening of photon current with respect to transport mean free time [35] are not be universally applicable. The theory, also known as the P_1 approximation, is only valid when the absorption coefficient is much lower than the scattering coefficient. Even when this condition is fulfilled, the predictions are inaccurate when a light source is near the target and for collimated sources (such as lasers) because the approximation cannot accommodate angular anisotropy [36]. Although attempts have been made by simplifying lasers to point sources in the tissue, computationally intensive MC methods still remain more accurate than the P_1 approximation [35].

An alternate approach known as the Kubelka-Munk (KM) theory can also be derived from the RTE [37] and is useful for rapid quantitative assessments [29]. Although the assumptions of KM theory include diffuse incident radiation and ignore regular reflection at boundaries, they have been used to quantify surface reflectance and model skin colours [38].

Further strategies such as the adding-doubling method [39] have been described but cannot construct accurate stochastic models as a function of optical properties. MC methods for biomedical optics have emerged as the best solution in these scenarios, albeit at the expense of computational load and time.

2.3 | Monte Carlo Simulations

MC simulations are the "gold standard" for modelling interactions between light and biological tissues, and testing procedures in biomedical photonics [5,40]. The transmission of light through tissues is complex due to the heterogeneous distribution of chromophores and the different refractive indices of the various layers.

In order to achieve a convergence to realistic results from stochastic methods, millions of interactions need to be accounted for. For interactions with $\geq 10^7$ rays, "brute force" MC simulations are impractical without variance reduction. This is achieved by importance sampling and ray splitting, which improves the efficiency and accuracy of the MC method. Importance sampling involves the propagation of rays in the specific direction or onto a particular surface of significance for the system. This improves sampling of the attenuated power by directing more rays (not power) towards the surface of interest. Ray splitting is used to enhance efficiency by splitting every interaction of a ray with an attenuating particle into four components: specular reflectance and transmittance, and scattered reflectance and transmittance. By also modelling absorption, the five components add up to the power of the incident photon. Variance reduction was implemented in our current study using TracePro.

One of the best known MC methods for biomedical optics in multi-layered tissues (MCML) [41] calculates the fraction of photon energy lost due to absorption using the absorption albedo ($(\mu_a)/(\mu_a + \mu_s)$). Scattering events were quantified using polar and azimuthal angles calculated from the Henyey-Greenstein phase function. The photons are eventually eliminated when reflected, or transmitted out of the tissue, or when their power drops below a predefined threshold. Generally, all MC model variants follow the same principles but can be applied to tissues modelled as two-layer models [42], seven layers [43] and nine layers [44], among others. MC methods have been used to quantify the interactions between light and blood [45], skin lesions [46], breast tumours [7], liver tissue [47], and for retinal oximetry [48]. MC methods have been improved by using scaling and perturbation for the detection of tumour-like heterogeneities [49] and parallel computation has been used to improve the speed and efficiency of the algorithm [50,51]. The use of MC methods to investigate transmission of light through tissues has been reviewed [52].

In biomedical optics, photons are treated as random samples whereas their absorption, scattering and transmission after interacting with chromophores and particles are physical processes. The optical properties of tissues are defined by the refractive index ($\hat{\eta}$), absorption coefficient (μ_a), scattering coefficient (μ_a) and anisotropy (g). The absorption coefficient and the refractive index define the material behaviour whereas the scattering coefficient and anisotropy influence the bulk scattering of light at a specific wavelength. The refractive index is defined in the current study as a complex index ($\hat{\eta} = \eta + ik$ where $k = (\lambda\mu_a)/(4\pi)$) [53]. The scattering and absorption coefficients determine the probability of attenuation events per unit path length and the inverse of mean-free-path (mfp) for attenuation occurrence. Both coefficients are defined in inverse units of length (cm^{-1} or mm^{-1}).

Once the absorbed fraction of the photon's energy is deducted, the remaining energy is attenuated based on the scattering distribution function (Henyey Greenstein phase function [41,53,54]) shown in Eq. 1, which is used in our MC calculations.

$$SDF = p(\theta) = \frac{1 - g^2}{4\pi(1 + g^2 - 2g\cos\theta)^{3/2}} \quad (1)$$

$$g = <\cos\theta> \Rightarrow \theta = \cos^{-1}(g) \quad (2)$$

The dimension-less anisotropy (g) is the average cosine of the scattering angle (Eq. 2). It represents the average scattering angle over numerous events [55]. Therefore, the variation in g dictates the scattering direction, with positive values indicating forward scattering, negative values indicating backscatter, and zero for isotropy [56].

3 | CONSTRUCTION OF HUMAN SKIN EQUIVALENTS

The HSEs in this study were prepared by the co-cultivation of dermal fibroblasts and primary keratinocytes [2], allowing the growth of skin tissue similar in structure to that observed *in vivo*, with comparable morphology, stratification, growth and response to stimuli (Figure 3).

Primary normal human dermal fibroblasts (NHDFs) (Promocel, UK) were cultured in Dulbecco's Modified Eagle's Medium, supplemented with 10% foetal bovine serum (FBS), 1% L-glutamine and 1% penicillin/streptomycin (all reagents from Thermo Fisher Scientific, UK). Primary normal human epidermal keratinocytes (NHEKs) (Promocell, UK) were cultured in KGM-Gold (Lonza, UK). Six-well polyester Transwell inserts (Corning Inc., USA) were coated with a layer of acellular collagen as an attachment substrate for the cellular collagen, preventing the overlying layers from contracting through the insert membrane, thus promoting a favourable micro-environment for the HSE model while regulating epidermal growth and proliferation [1]. The NHDFs were centrifuged at 220 RCF (relative centrifugal force) for 3 min and re-suspended in growth medium to a concentration of 3×10^5 cells/ml. We then mixed 1.5 ml of the cells with 15 ml of collagen and 3 ml of the resultant mixture was added to each Transwell insert. After incubation for 30 min at 37 °C in a 5% CO_2 atmosphere, the acellular collagen matrix set at the bottom of the Transwell insert and formed the basement membrane to support the skin model.

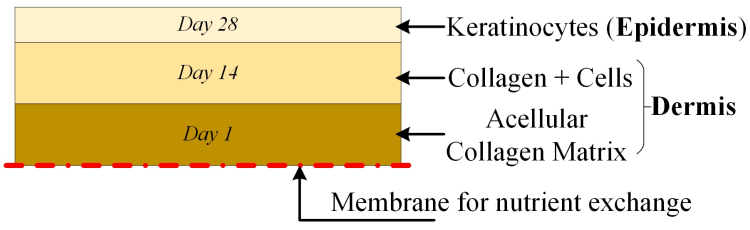

FIGURE 3 The acellular collagen matrix allows the proliferation of the dermis (from fibroblasts) and epidermis (from keratinocytes).

Having formed a basement membrane, the dermal cells were cultured for 2 weeks, replacing the medium every 2 days until the collagen was fully contracted. The NHEKs were then centrifuged at 220 RCF for 3 min and suspended in medium at a concentration of 2×10^6 cells/ml. The medium was removed from each Transwell and 100 μl of the NHEK suspension was aliquotted onto the surface. After incubation at 37 °C for 1 h in a 5% CO_2 atmosphere, 3 ml of cornification medium was added to each well to promote cellular interactions at the air-liquid interface. The medium was replaced every 2 days for 2 weeks until the keratinocytes had fully differentiated and the epidermis had formed over the dermal layer to form a full-scale HSE. However, the HSE samples lacked the chromophores melanin and haemoglobin found in real skin.

In this study, samples 1, 2, 7 and 8 are controls, untouched from the beginning of synthesis. All the other samples were subjected to mechanical stimuli for a different study, unrelated to optical measurements. Samples 1-6 contracted during synthesis, and were therefore considerably thicker than samples 7-12. Sample 5 was damaged during the mechanical experiments and was also infected.

4 | MONTE CARLO EVALUATION OF TWO-LAYER SKIN MODEL

MC methods were applied to stochastic models in order to quantify the degree of absorption and scattering over millions of instances. The methods converge on a realistic result at the expense of computational load and time. The simulations in this study were implemented using the ray-tracing package TracePro, which provides all the tools necessary to arrange the layers, input their optical parameters and arrange the detector and light sources. Two ray-tracing methods were available: Analysis mode and Simulation mode. Analysis mode allows the graphical representation of rays and hence the visualisation of the interactions, but it is limited by the availability of computer memory. For example, tracing ≈800,000 rays uses ≈48 GB of random access memory. This mode is unsuitable for tracing millions of rays, as required in our investigation. We therefore used Simulation mode, in which the history of ray traces and interactions are stored on the hard drive during the course of the simulation. Sufficient hard drive space allows the tracing of millions of rays.

The light sources were modelled with reference to laser diode modules CPS980 and CPS670F (Thorlabs Inc., USA), which were used in the experiments. The beam geometry was simulated according to the manufacturer's specifications, with powers of 4.64 and 4.1 mW for the red and NIR lasers, respectively. The model featured two coincident, semi-infinite slabs as reported elsewhere[42,57,60]. In these models, light is transmitted through the layers, experiencing absorption and scattering, until a portion of it reaches the detector. Finally, two hemispheres were placed around the model to measure the forward and backward scattering.

Having set up the source and detector (5.2 μm^2 pixels, 1280×1024 resolution), the geometry and optical properties were defined (Table 1 and 2). The thickness of the layers in the model is a key factor that influences photon interactions. If the

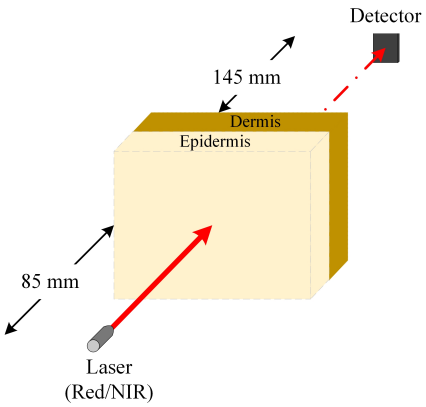

FIGURE 4 Light attenuates as it interacts with the layers of a skin model and a portion of it reaches the detector. The forward scatter and backscatter are quantified using two hemispheres (not shown), allowing us to quantify the absorbed energy as well.

TABLE 1 The optical properties used for the epidermis and dermis remained constant throughout the study. The absorption coefficients are scaled from Salomatina *et al.* [68] and scattering coefficients are adopted from Tuchin *et al.* [6].

Layer	λ **(nm)**	μ_a **(cm^{-1})**	μ_s **(cm^{-1})**	g	n
Epidermis	577	3.9	120	0.78	1.335
	633	2.6	107	0.79	
	670	2.6	-	**0.8** †	
	920	0.7	-	**0.8**	
	970	0.6	-	**0.8**	
	1020	0.4	-	**0.8**	
Dermis	577	2.2	205	0.78	1.37
	633	1.5	187	0.82	
	670	1.5	-	**0.8**	
	920	0.8	-	**0.8**	
	970	0.8	-	**0.8**	
	1020	0.7	-	**0.8**	

†The anisotropy factor of 0.8 is taken from Salomatina *et al.* [68].

absorption and scattering coefficients remain constant, greater thickness lengthens the optical path of each photon because there are more scattering events, while increasing the probability of eventual absorption. In some cases, the thickness of skin in its entirety is available (as is the case for HSE samples). We used a previously published epidermis-to-dermis thickness ratio (E/D) [70–72], based on ultrasound experiments that give us the palmar (inner side of the hand) and dorsal (outer side of the hand) thicknesses in this study (Table 2).

The thickness of the palmar and dorsal measures used in the simulations were averaged over ultrasound measurements that were collected *in vivo* from 17 participants at the Great Western Hospital (Swindon, UK) using an 18-MHz probe. The thickness of the HSEs was measured in the laboratory as described in Section 5. We estimated that the epidermis contributed 10.4% to

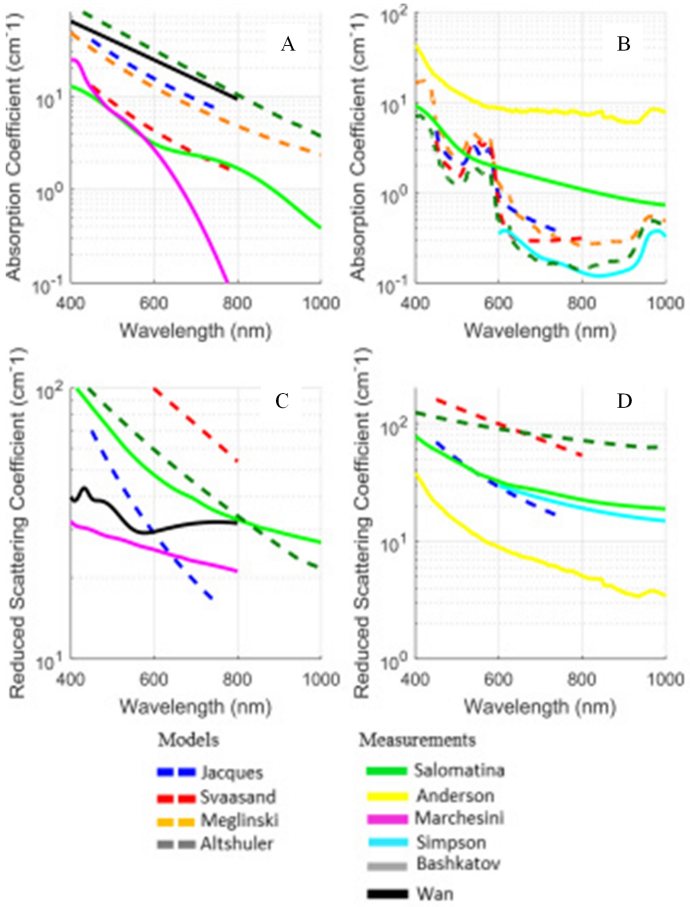

FIGURE 5 The attenuation coefficients (μ_a, μ_s) of the epidermis (A, C) and dermis (B, D) in this study are derived from published values [13,29,61–68]. Reprinted from Ref. [69] with permission [OSA].

the thickness of the full model based on ultrasound data and the E/D metric. This was later verified by histological analysis. Models Sim1 – Sim4 (Table 2) were run using combinations of red and NIR sources, with dorsal and palmar skin models. The same approach was used for models HSE_Sim1 – HSE_Sim12 (Table 2). All surfaces not perpendicular to the beam direction (the side surfaces of the model) were made perfect absorbers in order to treat the layers as a semi-infinite slab.

The final step in setting up the simulations was the assignment of the optical properties to the epidermis and dermis. Given that the HSE sample has no melanin or haemoglobin in its layers, the light attenuation depends mainly on scattering. Because the variation of properties overall is almost 100-fold [69], the choice of properties was based upon literature data [13,29,61–68].

Salomatina *et al* [68] measured the absorption coefficient of excised epidermis using inverse MC methods. These measures were our first choice because the quantification of melanin absorption is low, haemoglobin absorption is absent and the overall absorptive behaviour is comparable to the HSE, which lacks chromophores. The absence of these properties is attributed to the handling and washing of the skin samples *in vitro*. Estimating optical properties from measurements of excised and washed samples, rehydrated with saline solution [68] has the disadvantages of altering the chromophore content and distribution. However,

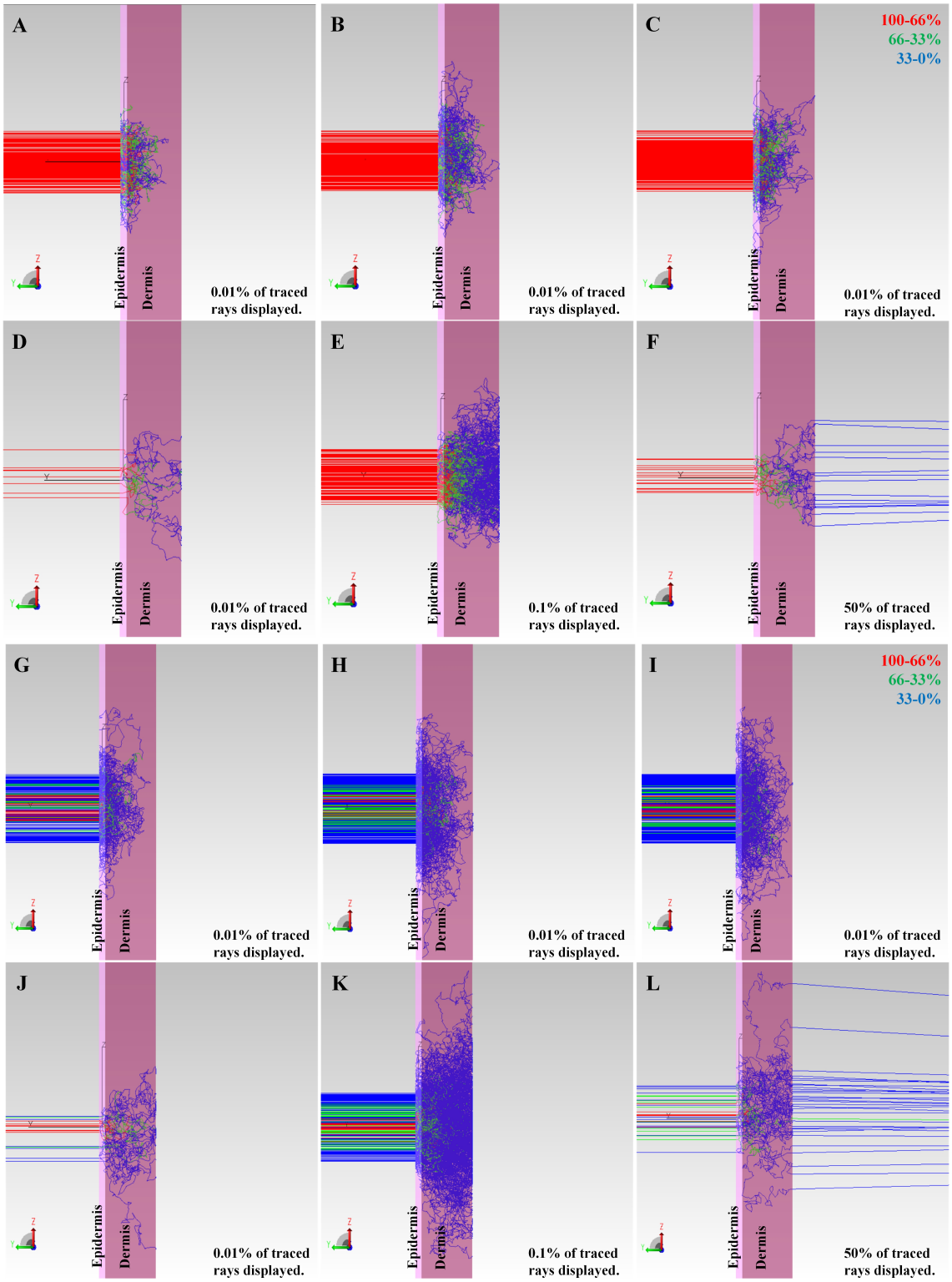

FIGURE 6 The images show a palmar skin model irradiated with red (A–F) and near-infrared (G–L) light. We traced a total of ≈700,000 rays. The light interacts consecutively with the epidermal and dermal surfaces of the model, which are perpendicular to the beam direction. A total flux of 1.71 nW red light and 71.8 nW near-infrared light is incident on the detector.

the properties were in agreement with the mathematical model described by Svaasand *et al*[61], and 10-fold lower than the improved model presented by Altshuler *et al*[63] (Fig. 5 A). The absorption coefficient estimated by Salomatina *et al*[68] was also four times lower than the value reported by Jacques[13], based on neonatal skin samples for measurement of baseline values including all the anatomical features except high concentrations of melanin. However, these measures take fewer factors into account and do not consider the impact of water content. Therefore, we scaled the $\mu_{a,epi}$ estimates from these previous reports[68] [63] by a factor of 10.

When comparing the absorption coefficients for the dermis ($\mu_{a,derm}$), major absorption peaks due to haemoglobin are missing in the Salomatina *et al*[68] and Anderson[29] estimates, a trend we elected to keep for our study to ensure that absorption could be quantified for comparison at a later stage. Accordingly, $\mu_{a,derm}$ was scaled by a factor of 10, similar to $\mu_{a,epi}$, making the measures comparable to those reported by Anderson[29] based on reflectance and transmittance methods followed by KM theory. In summary, we compared the contributions of the chromophores, selected the values reported by Salomatina *et al*[68] and multiplied by 10 to accommodate the contributions of melanin, while disregarding the variable dermal absorption due to haemoglobin.

For the scattering coefficients, we adopted a different approach based on previous interpretations[69]. The tissue is a turbid medium characterised by much higher scattering than absorption ($\mu_s >> \mu_s$). Therefore, the coefficients must reflect this difference as well. The optical model of skin, including its chromophores, was analysed using an inverse MC method and KM theory[6]. The study characterised the scattering behaviour of the two layers, including the contributions of melanin and haemoglobin. We used the corresponding $\mu_{s,epi}$ and $\mu_{s,derm}$ values directly[6].

In summary, the hybrid optical properties representing our skin model for MC methods include the scaled contribution of melanin for absorption, as well as melanin and haemoglobin for scattering. Our motive was to compare the simulation and HSEs in terms of transmittance, accounting for the contribution of the two major chromophores. The hybrid optical model is summarised in Table 1.

5 | OPTICAL INVESTIGATIONS

The HSEs ($n = 12$) were cultured in Transwell scaffolds with a membrane to support the layers and allow the transfer of nutrients. The samples were mounted on a scaffold and held vertically along the path of a laser beam produced by CPS670F ($\lambda_{CW} = 674$ nm) and CPS980 ($\lambda_{CW} = 978$ nm) laser diode modules and a power meter (Lasermet ADM 1000) to record the transmitted power. The central wavelengths (λ_{CW}) and power stability of the lasers were calibrated prior to shipment and were confirmed in the laboratory before experiments with the HSEs.

Optical measurements were performed by removing HSEs from the culture medium at the end of the culture period and discarding the surplus medium. Four samples were labelled as controls (1, 2, 7, 8) and the other eight were subjected to mechanical

stimuli with a pin for a different set of experiments. Each of these samples was then placed in a custom holder and mounted on a rail, directly in front of the laser source. Once alignment was confirmed between the source, sample and power meter, we measured the power transmitted through the sample.

Each sample was placed 85 mm from the laser diode module, with the power meter detector placed 145 mm behind the sample. Any light that did not pass through the sample to reach the detector was either scattered or absorbed. The optical transmission of each sample was assessed at red and NIR wavelengths. Due care was taken when the samples were held vertically in the path of the laser beam to avoid significant movement when measuring linear transmission, but minor movements and variations in thickness were unavoidable.

The thickness of each sample was measured in the laboratory when the optical experiments were complete, and was used to set up the simulation models. In order to compare and validate the thickness variations in the samples, the samples were prepared for haematoxylin and eosin (H&E) staining by washing with saline solution. The thickness was measured before staining and histological analysis because the preparation method causes sample dehydration and this reduces the thickness of each layer (Figure 7 and 8). The thickness of all 12 samples is shown in Table 2 . The mean sample thickness was 1.11 mm and the standard deviation was 0.77 mm.

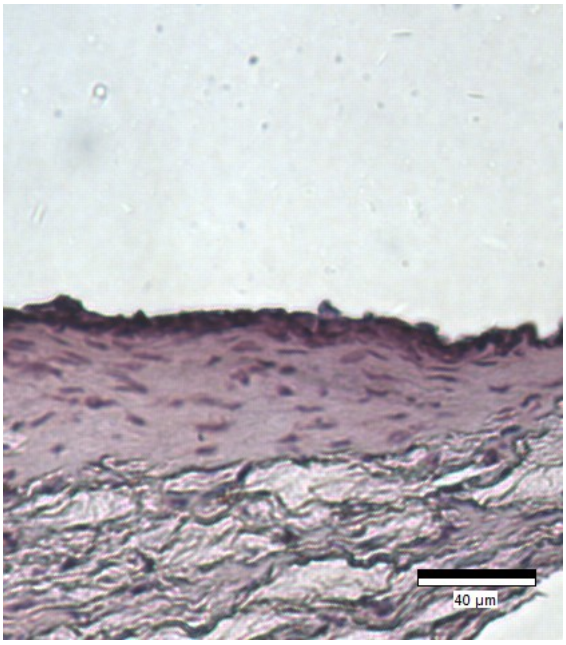

FIGURE 7 Histological analysis of one of the HSEs shows clearly formed epidermis and dermis. The sample is significantly thinner than the measured thickness due to dehydration during the preparation for histological staining.

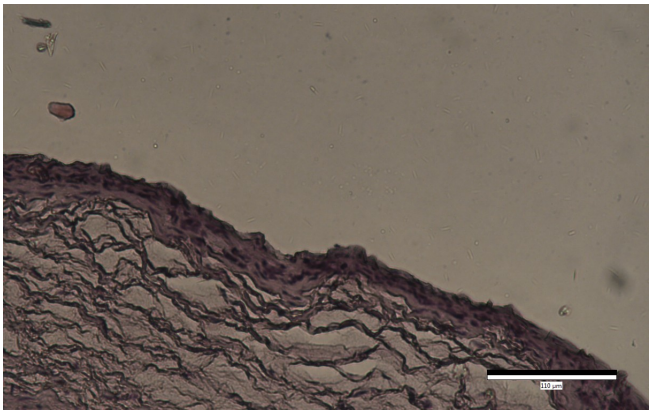

FIGURE 8 Enlarged view of an HSE sample after haematoxylin and eosin (H&E) staining shows clearly defined layers, providing evidence of the layer-by-layer synthesis.

6 | RESULTS AND DISCUSSION

The primary objective of this investigation was to compare the optical properties of simulated human skin models with HSEs representing real human skin. In this section, we (1) present the results of simulations using models differing in layer thickness and (2) compare the simulations to experimental transmission measurements.

6.1 | Monte Carlo simulations

Although the models were tested in Simulation mode, we also used Analysis mode with fewer rays for illustration purposes. We picked the thicker palmar skin model, due to the possibility of more interactions with the red (Fig. 6 A-F) and NIR (Fig. 6 G-L) wavelengths.

As the light travelled through the layers, it was attenuated by absorption and scattering events representing interactions between the tissue and photons. These processes occurred in addition to surface reflection and refraction due to variations in the refractive indices of the samples. The surfaces and their interactions with light (Fig. 6) are relevant to all the simulations (Table 2) in this study.

- Fig 6 (A) and (G) reveal interactions between rays and the surface of the epidermis facing the source. The scattering data showed that the light penetrates the dermis before subsequent scattering events divert the rays back towards the epidermis or perpendicular the model. The rays that exit through the incident surface of the epidermis were accounted for by measuring the backscatter in the simulation.
- Fig 6 (B) and (H) illustrate interactions between incident rays and the epidermal surface at the epidermisdermis interface.

TABLE 2 Monte Carlo simulations of human skin, illustrating some common inferences such as greater transmittance in the near-infrared wavelength and thicker skin models restricting transmission in the red (λ = 674 nm, flux = 4.64 mW) and near-infrared (λ = 978 nm, flux = 4.1 mW) wavelengths. Approximately 12×10^6 rays were traced at both wavelengths 5.2 μm^2 detector pixels were set at 1280×1024 resolution. The simulation results for HSE 4 and 11 were identical to 5 and 10, respectively, because the thickness in each case was also identical.

Simulation	λ (nm)	Detector			Forward Scatter (mW)	Back-scatter (mW)	Model Layer Thickness (E, D; mm)
		Rays	Transmitted Power (μW)	Maximum Irradiance (W/m^2)			
Sim1	674	1977	0.11	8.20	0.18	1.64	0.24, 2.04
Sim2	978	3019	0.23	22.9	0.36	2.11	(Dorsal)
Sim3	674	730	0.02	5.30	0.02	1.52	0.4, 3.3
Sim4	978	1368	0.06	15.8	0.10	2.13	(Palmar)
HSE_Sim1	674	1479	0.13	8.60	0.22	1.54	0.22, 1.88
	978	2045	0.41	24.4	0.41	1.99	
HSE_Sim2	674	1607	0.15	14.0	0.25	1.55	0.21, 1.79
	978	2138	0.45	24.4	0.45	1.98	
HSE_Sim3	674	1787	0.18	9.20	0.29	1.56	0.2, 1.7
	978	2315	0.50	26.4	0.49	1.98	
HSE_Sim5	674	1998	0.21	9.40	0.33	1.57	0.19, 1.61
	978	2455	0.54	26.6	0.54	1.97	
HSE_Sim6	674	2414	0.30	13.9	0.49	1.59	0.16, 1.34
	978	2820	0.71	27.5	0.71	1.94	
HSE_Sim7	674	4192	0.91	22.9	1.45	1.55	0.06, 0.49
	978	4427	0.97	33.6	1.56	1.67	
HSE_Sim8	674	5211	1.29	23.6	1.71	1.50	0.07, 0.6
	978	5582	1.31	38.6	1.76	1.58	
HSE_Sim9	674	364553	123	250	2.78	1.06	0.02, 0.18
	978	365488	112	227	2.58	1.03	
HSE_Sim10	674	159362	53.3	137	2.61	1.18	0.03, 0.22
	978	160088	48.5	175	2.46	1.16	
HSE_Sim12	674	66397	21.8	86.2	2.43	1.29	0.03, 0.27
	978	66914	20.0	124	2.32	1.27	

- Fig 6 (C) and (I) reveal interactions between incident light and the dermal surface at the epidermis-dermis interface. In the four images (B), (C), (H) and (I), the number of scattering events increases due to the forward scattering nature ($g>0$) and greater scattering coefficient of the dermis.
- Fig 6 (D) and (J) reveal interactions between incident light and the dermal surface facing the detector. This is the surface from which the light exits the skin model. The possible fates of light rays at this surface are refraction (back into the model) or exit. The energy exiting the model and not incident on the detector is considered forward scatter. This measure, along with the amount of backscatter, is used to measure the amount of power absorbed by the skin model.

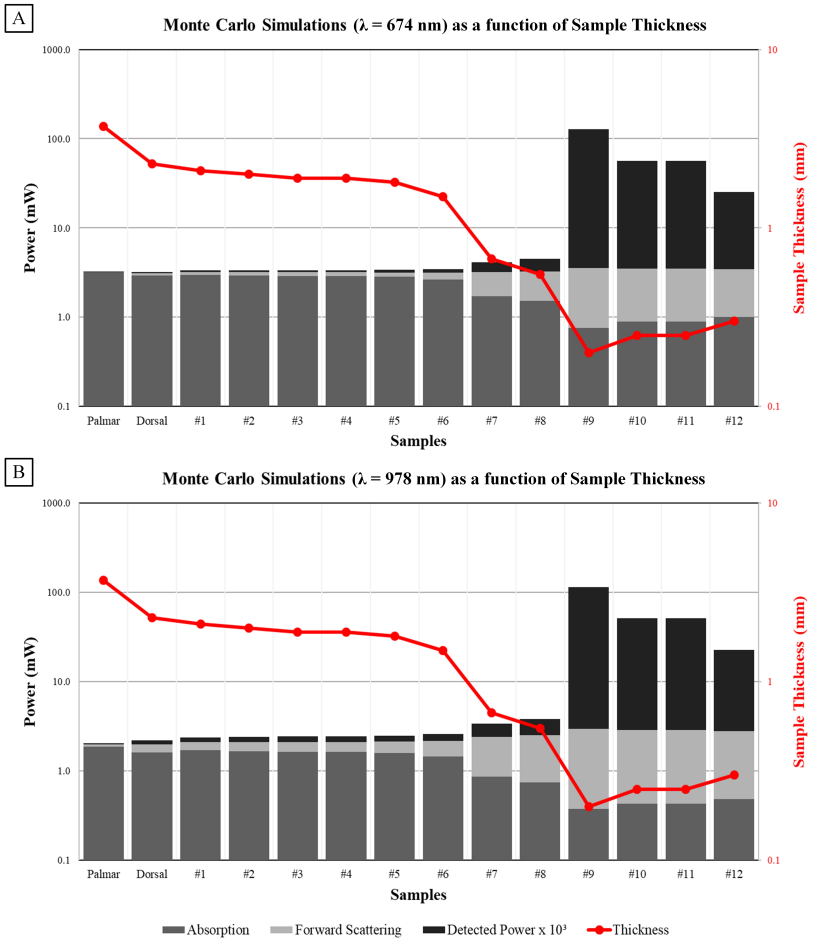

FIGURE 9 The absorption by the skin layers, forward scattering from the skin model and the power detected on the detector in the simulation environment are evidentially related to thickness. The detected power measurements are scaled to mW from μW to show the trend on the same scale for comparison. All the values represented here are also listed in Table 2.

- Fig 6 (E) and (K) reveal a greater percentage of rays interacting with final surface of the model, facing the detector. In both images, we observed the dissipation of energy with increasing depth. Although more obvious in (E), the principle holds true for both wavelengths.
- Fig 6 (F) and (L) show 50% of the traced rays, and their paths from the source to the detector. Along this path, attenuation occurred as absorption or scattering. In agreement with earlier reports, greater power is transmitted in the NIR range. Using the palmar skin model, 1.71 nW of power reached the detector in the red waveband, but ≈42 times as much reached the detector in the NIR waveband.

The ray-tracing results of the skin models in Simulation mode are presented in Table 2, and the interactions are sumarised in Fig. 9. When the sample thickness is > 0.3 mm (Sim1–HSE_Sim8), the transmission of NIR rays is unquestionably greater than red. When the thickness is < 0.3 mm, more NIR than red rays are detected but the power reaching the detector is similar for both wavelengths. Additionally, in the simulation and the experiments, we were able to 'see' the laser beam as opposed to

a scattered speckle-like pattern. Therefore, we conclude that thin HSE samples (< 0.3 mm) behave like neutral density filters, such that more light is absorbed than scattered, whereas the opposite applies for thicker samples due to the increased likelihood of interactions. When the thicker palmar skin model was irradiated with red light, 3.2 mW (67%) of the power was absorbed, whereas the thinner HSE_Sim12 model irradiated with NIR light absorbed only 12% of the incident power. The simulation of the thinnest sample (HSE_9) forward scattered 55% of the red light and 60% of the NIR light.

In contrast to the predictable effects on forward scatter, there was much greater variability in terms of backscatter. In thicker samples (> 0.3 mm), 31-34% of the red light was backscattered compared to 38-52% of the NIR light. The thinner samples backscattered less than 30% of the incident light at both wavelengths, with the exception of sample HSE_12 at NIR wavelengths.

More light was absorbed by the thicker samples. Given optically identical layers (i.e. the same optical properties), forward scattering and the power of transmitted light increased for the thinner samples (Fig. 9). The number of rays incident on the detector was also attenuated by the skin model at a given thickness and set of optical properties [65]. We clearly observed a change in properties and trends at thickness below 1 mm.

6.2 | Transmission Measures

The experimental design allowed us to quickly and effectively measure the transmission of light through the samples, and compare the simulation results (Fig. 10). Three measurements were taken per sample and the results were stable and dependable. MC simulations were repeated using the unscaled μ_a values reported by Salomatina *et al.* [68] for comparison. The unscaled values, although not accommodating the chromophores in the skin [69], allowed us to consider a scenario of lower or negligible melanin and haemoglobin levels in the skin, as is the case with HSEs.

Overall, the simulated and measured power at the detector revealed a linear relationship between simulated and measured transmittance for the first eight samples (Fig. 11 A,B). This held true for both the red and NIR lasers. However, when the sample thickness was lower ($d \leq 0.3$ mm), the comparison between measurements changed to a logarithmic relationship with a poorer fit (Fig. 11 C,D). We infer that the measured and simulated transmitted power is poorly described for the thinnest of the skin layers. However, with only four data points, we cannot make a generalised conclusion regarding these thinner samples.

We also compared the variability of the measurements ($P_{measured}/P_{sim}$) with the thickness of the samples (Fig. 11 E,F). The exponential relationship with the thickness of the samples (and skin models) indicated a lower frequency of absorption and scattering events in the optical path.

Visually, a cluster of measures was seen in the thickest samples ($d > 1$ mm) and when analysing this cluster, the fit to the exponential relationship was better. We conclude, within the experimental limits of this study, that the variability of the samples and their transmission as a function of thickness is weakly related in thinner samples ($d < 1$ mm). This may be due to the shorter

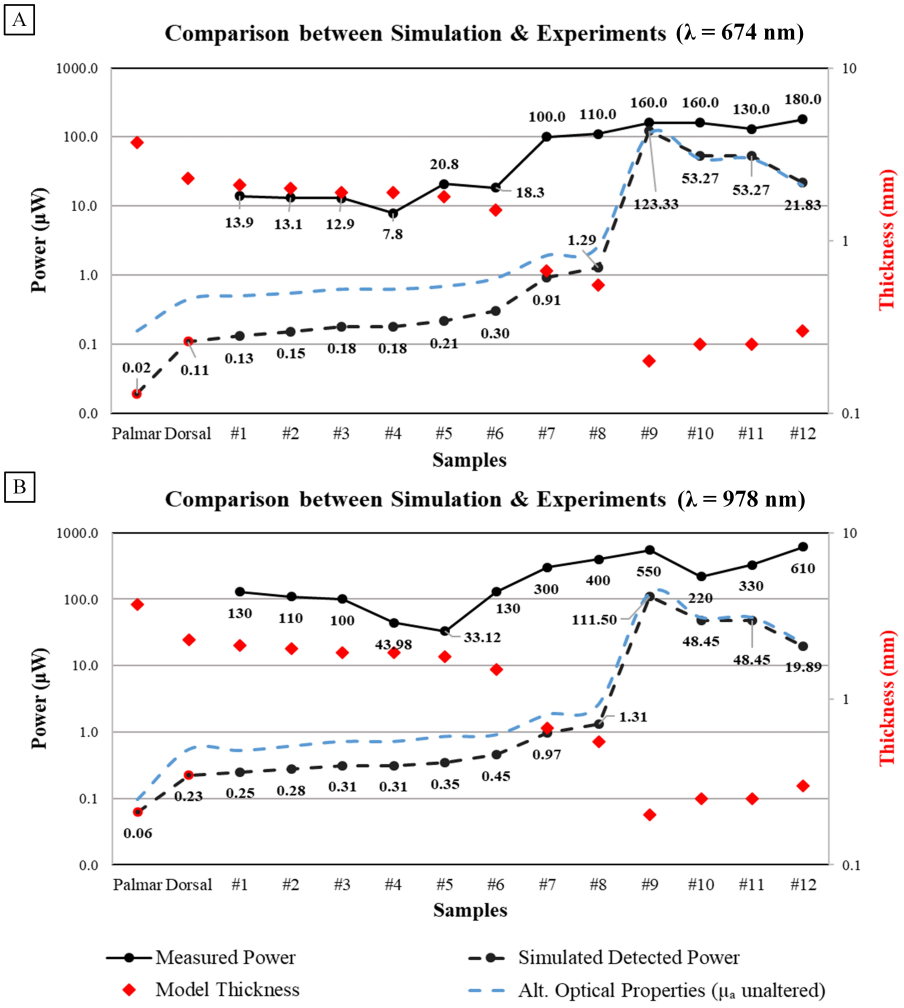

FIGURE 10 The comparison between simulation and experimental measures shows exponentially increasing differences as the sample becomes thinner ($P_{measured}/P_{sim}$). The detected power of simulations with higher values of μ_a (-●-) is lower than μ_a reported by Salomatina *et al*[68] (blue dashed line) until thickness of the sample falls below 0.5 mm. For these thinner samples, the detected power is almost identical.

optical path and the lower frequency of absorption and scattering events. The simulation and experimental results show that the linear relationship holds true when $d \geq 0.5$ mm, but the exponential trend is more appropriate when $d > 1$ mm.

The most important inferences of this study were drawn from the comparison shown in Fig. 10 , in which the simulated and measured detected power values are shown as black lines (-●-, - -). The simulated powers were based on the palmar and dorsal skin models and the final HSE model. The trends were similar for both plots. Overall, the trends also varied inversely with the thickness of the samples. The detected power values for sample #9 were highest because this was the thinnest of the samples. A slight increase in detected power was seen overall when the unscaled optical properties reported by Salomatina *et al.*[68] were used, which underestimated the absorption effect of the chromophores. The difference between the measured power and

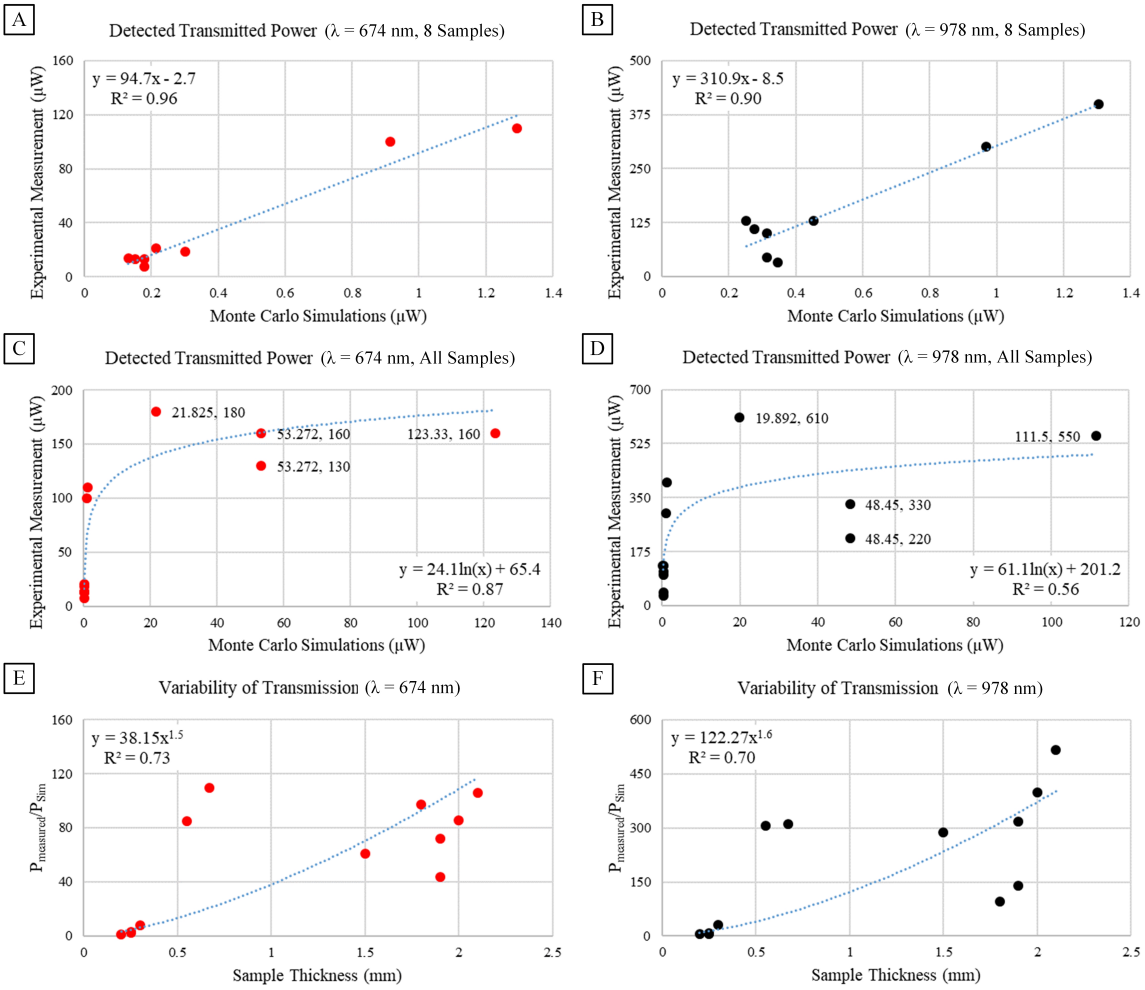

FIGURE 11 For the first eight samples (thickness >0.5 mm, the linear relationship (A,B) best fits the data comparing the measured and simulated transmissions. The detected power, however, shifts to a poorer fit and a logarithmic relationship when including all samples. The four data points with callouts (C,D) correspond to thinner samples (<0.5 mm). Finally, an exponential increase (E,F) in detected transmission is seen in samples thinner than 1 mm.

simulated power can be qualitatively explained by the absence of chromophores in the HSEs, thereby allowing experimental measures to be higher than the simulated results.

6.3 | Sources of Error

Due to the nature of this pilot study, we must account for potential sources of error in order to improve the analysis of HSE samples in the future. The simulations consider an ideal scenario for source and detector functionality, and the optical properties described in the literature vary over two orders of magnitude [69].

Histological analysis provides an accurate method to determine geometric thickness but the preparation of histological specimens alters the moisture content in the layers and their geometric arrangements. Furthermore, histological preparation often

washes out key chromophores that are abundant in the skin *in vivo*. Therefore, we relied on measurements with calipers in the laboratory and compared histological samples assuming the degree of dehydration remained constant. This gave us reliable measurements for the simulation. The handling and preparation of the experimental samples contributed to the variability of the measurements. Another qualitative aspect to consider is the integrity of the layers in the sample when held vertically for the transmission experiments. The samples are very thin and can slip, slide or shift when held in the path of the laser beam. This could alter the optical path length because the thickness *in situ* may differ from the initial measurement. We assumed that such changes would have a negligible effect in our experiments.

When comparing HSEs with *in vivo* skin layers, we deduce that the changes to physical parameters such as μ_a and μ_s explain the manifold variation in the detected power (Fig. 10). These physical properties are based on the presence and distribution of specific chromophores, thickness of the layers and macroscopic composition of the tissues. As we have not observed a significant change in the detected power due to the variation of the absorption coefficient (μ_a), reduced scattering by the HSE sample can be deduced as the contributor to the increase of measured power at the detector in the experiments. We speculate that anatomical variations could be a contributing factor to this. The epidermis layer of the human skin consists of cells other than self-renewing keratinocytes. These include melanocytes, lymphocytes, Merkel cells and Langerhans cells, each performing specific functions. Considering the dermis layer, in addition to blood, nerves and lymphatics are also present in human skin. The density of the collagen fibre network in dermis layer also varies depending on the parts of the body, contributing to interaction with light.

7 | CONCLUSIONS AND FUTURE WORK

The diverse applications of HSEs require the development of models with properties that match *in vivo* skin as closely as possible. Here we have presented a methodology for optical comparisons in a pilot study that brings together (1) MC simulations of light interacting with skin and (2) the direct investigation of light transmittance through HSEs.

The simulation combined the optical properties of the epidermis and dermis (including the contributions or lack thereof of melanin and haemoglobin) with the effect of varying the sample thickness. The experiments provided a quick and simple method to measure the transmittance of red and NIR light through the samples. The difference in transmittance between the simulations and experiments revealed the effect of the absence of chromophores in the HSE samples, but the trend remained comparable in samples thicker than 0.5 mm. When the thickness of the sample is < 0.5 mm, the transmittance of red and NIR light became comparable, with the samples acting like neutral density filters and showing minimal absorption.

Looking ahead from this pilot study, we would like to make some suggestions to facilitate future investigation of HSEs. In addition to the results and inferences of the study, we recommend application of integrating spheres and inverse optical properties estimation methods. Other Monte Carlo platforms (like MCML, Monte Carlo eXtreme) can be applied for possible improvements

in processing times, portability and applicability/accessibility. Water in the HSEs also play a role in determining the absorption of light. In order to better quantify this contribution, transepidermal water loss (TEWL) methods can be employed. Human skin equivalents hold great potential in a multitude of applications, as discussed, and optical investigation is a good and dependable method of assessment.

ACKNOWLEDGMENTS

We would like to thank Ms Paulami Ray, Dr Amit Yadav and Prof Edik Rafailov (AIPT, Aston University), and Dr Mark Finnis (Cranfield University) for their support with laboratory facilities at various stages of the research. We are grateful to Dr Elizabeth Price, Mrs Catherine Lewis-Clarke and the staff of the Radiology Department at Great Western Hospital (Swindon, UK) for their assistance and support with the ultrasound measurements. We also acknowledge Dr Richard M Twyman for assisting with manuscript editing.

Author contributions

The study was designed by AK and DJ, assisted by BM, SJ and MR. AK, BM and DJ conducted the optical experiments on the HSEs. MC simulations in TracePro were carried out by AK. BM and SJ synthesised the HSE samples *in vitro* and BM acquired the microscopic images of the samples. JH collected the ultrasound measurements used in the study. The manuscript was written by AK and BM, with contributions from the other authors.

Financial disclosure

None reported.

Conflict of interest

The authors declare no potential conflict of interests.

References

[1] F. Andriani, A. Margulis, N. Lin, S. Griffey, J. A. Garlick, *The Journal of Investigative Dermatology* **2003**, *120* (6), 923–931.

[2] M. W. Carlson, A. Alt-Holland, C. Egles, J. A. Garlick, *Current Protocols in Cell Biology* **2008**, *41* (1), 19.9.1–19.9.17.

[3] C. M. A. Reijnders, A. van Lier, S. Roffel, D. Kramer, R. J. Scheper, S. Gibbs, *Tissue Engineering Part A* **2015**, *21* (17-18), 2448–2459.

[4] H. Mertsching, M. Weimer, S. Kersen, H. Brunner, *GMS Krankenhaushygiene interdisziplinar* **2008**, *3* (1).

[5] S. A. Prahl, M. Keijzer, S. L. Jacques, A. J. Welch, *Dosimetry of Laser Radiation in Medicine and Biology* **1989**, *5*, 102–111.

[6] V. V. Tuchin, S. R. Utz, I. V. Yaroslavsky, *Optical Engineering* **1994**, *33* (10).

[7] G. M. Palmer, C. Zhu, T. M. Breslin, F. Xu, K. W. Gilchrist, N. Ramanujam, *Applied Optics* **2006**, *45* (5), 1072–1078.

[8] A. Hasan, *Tissue Engineering for Artificial Organs*, Wiley-VCH Verlag GmbH & Co. KGaA, Weinheim, **2017**.

[9] Z. Zhang, B. B. Michniak-Kohn, *Pharmaceutics* **2012**, *4* (1), 26–41.

[10] E. R. Shamir, A. J. Ewald, *Nature Reviews Molecular Cell Biology* **2014**, *15*, 647–664.

[11] V. V. Tuchin, *Physics - Uspekhi* **1997**, *40* (5), 495–515.

[12] G. V. G. Baranoski, A. Krishnaswamy, *Revista de Informática Teórica* **2004**, *11* (1), 33–62.

[13] S. L. Jacques, *Physics in Medicine and Biology* **2013**, *58* (11), R37–R61.

[14] T. Vo-Dinh (Ed.), *Biomedical Photonics Handbook*, CRC Press, Boca Raton, Florida, USA, **2002**.

[15] V. V. Tuchin, *Tissue Optics: Light Scattering Methods and Instruments for Medical Diagnosis 2nd ed.*, SPIE (The Society of Photo-Optical Instrumentation Engineers), **2007**.

[16] C. Boudoux, *Fundamentals of Biomedical Optics*, Blurb Incorporated, **2016**.

[17] J. A. McGrath, R. A. J. Eady, F. M. Pope, *Anatomy and organization of human skin.*, T Burns, S Breathnach, N Cox, C Griffiths (Eds:), Blackwell Science Ltd Oxford, **2004**, pp. 3.1–3.15.

[18] C. Allombert-Blaise, S. Tamiji, L. Mortier, H. Fauvel, M. Tual, E. Delaporte, F. Piette, E. M. DeLassale, P. Formstecher, P. Marchetti, R. Polakowska, *Cell Death and Differentiation* **2003**, *10* (7), 850–852.

[19] P. A. J. Kolarsick, M. A. Kolarsick, C. Goodwin, *Journal of the Dermatology Nurses' Association* **2011**, *3* (4), 203–213.

[20] W. Paul, C. Sharma in *Advances in Wound Healing Materials: Science and Skin Engineering*, Smithers Rapra, **2015**, chapter 3, pp. 25–34.

[21] M. R. Wiles, J. Williams, K. A. Ahmad in *Essential of Dermatology for Chiropractors*, Jones and Bartlett Publishers, **2010**, chapter 3, pp. 29–32.

[22] J. Bensouilah, P. Buck in *Aromadermatology: Aromatherapy in the Treatment and Care of Common Skin Conditions*, Radcliffe, Oxford, **2006**, chapter 1, pp. 1–11.

[23] T. M. Kolodka, J. A. Garlick, L. B. Taichman, *Proceedings of the National Academy of Sciences of the United States of America* **1998**, *95* (8), 4356–4361.

[24] M. A. E. Abdallah, G. Pawar, S. Harrad, *Environment International* **2015**, *84*, 64–70.

[25]

[26] M. Jannasch, F. Groeber, N. W. Brattig, C. Unger, H. Walles, J. Hansmann, *Experimental Parasitology* **2015**, *150*, 22–30.

[27] A. De Breij, E. M. Haisma, M. Rietveld, A. El Ghalbzouri, P. J. Van Den Broek, L. Dijkshoorn, P. H. Nibbering, *Antimicrobial Agents and Chemotherapy* **2012**, *56* (5), 2459–2464.

[28] G. Sriram, M. M. Dykas, S. Ramasamy, K. Poddar, V. Krishnan-Kutty, A. Patra, T. Venkatesan, M. Bigliardi-Qi, P. L. Bigliardi, *Materials Today* **2016**, *19* (3), 178–179.

[29] R. R. Anderson, J. A. Parrish, *The Journal of Investigative Dermatology* **1981**, *77* (1), 13–19.

[30] N. M. Maughan, J. W. Moody, D. R. Miller, *Journal of Biomedical Optics* **2013**, *18* (10), 105007 1–6.

[31] A. Jubran, *Intensive Care Medicine* **2004**, *30* (11), 2017–2020.

[32] S. Chandrasekhar, *Radiative transfer*, Dover Publications, Inc. (New York, NY), **1960**.

[33] M. Wolf, K. von Siebenthal, M. Keel, V. Dietz, O. Baenziger, H. U. Bucher, *Physiological Measurement* **2000**, *21* (4), 481–491.

[34] J. M. Steinke, A. P. Shepherd, *Journal of the Optical Society of America A* **1988**, *5* (6), 813–822.

[35] L. V. Wang, H. Wu in *Biomedical Optics: Principles and Imaging*, John Wiley & Sons, Inc, **2007**, chapter 5, pp. 83–118.

[36] V. Venugopalan, J. S. You, B. J. Tromberg, *Physical Review E* **1998**, *58* (2), 2395–2407.

[37] C. Sandoval, A. D. Kim, *Journal of the Optical Society of America A* **2014**, *31* (3), 628–636.

[38] M. Doi, S. Tominaga, in *Proceedings of SPIE 5008, Color Imaging VIII: Processing, Hardcopy, and Applications*, (Eds: Reiner Eschbach, Gabriel G. Marcu), SPIE, **2003**, pp. 221–228.

[39] S. A. Prahl, M. J. C. van Gemert, A. J. Welch, *Applied Optics* **1993**, *32* (4), 559–568.

[40] T. Binzoni, T. S. Leung, A. H. Gandjbakhche, D. Rüfenacht, D. T. Delpy, *Physics in Medicine and Biology* **2006**, *51*, L39–L41.

[41] L. Wang, S. L. Jacques, L. Zheng, *Computer Methods and Programs in Biomedicine* **1995**, *47* (2), 131–146.

[42] D. Yudovsky, L. Pilon, *Applied Optics* **2009**, *48* (35), 6670–6683.

[43] I. V. Meglinskii, *Quantum Electronics* **2001**, *31* (12), 1101–1107.

[44] T. Maeda, N. Arakawa, M. Takahashi, Y. Aizu, *Optical Review* **2010**, *17* (3), 223–229.

[45] H. Nilsson, G. E. Nilsson, in *Proceedings in SPIE 3252, Optical Diagnostics of Biological Fluids III*, (Eds: Alexander V. Priezzhev, Toshimitsu Asakura, J. D. Briers), SPIE, **1998**, pp. 44–53.

[46] S. V. Patwardhan, A. P. Dhawan, P. A. Relue, *IEEE Transactions on Biomedical Engineering* **2005**, *52* (7), 1227–1236.

[47] S. Kumari, A. K. Nirala, *Optik - International Journal for Light and Electron Optics* **2011**, *122* (9), 807–810.

[48] S. Chen, J. Yi, W. Liu, V. Backman, H. F. Zhang, *IEEE Transactions on Biomedical Engineering* **2015**, *62* (9), 2308–2315.

[49] C. Zhu, Q. Liu, *Journal of Biomedical Optics Letters* **2012**, *17* (1), 010501 1–4.

[50] E. Alerstam, W. C. Y. Lo, T. D. Han, J. Rose, S. Andersson-Engels, L. Lilge, *Biomed. Opt. Express* **2010**, *1* (2), 658–675.

[51] F. Cai, S. He, *Journal of Biomedical Optics* **2012**, *17* (4), 1–4.

[52] C. Zhu, Q. Liu, *Journal of Biomedical Optics* **2013**, *18* (5), 50902 1–13.

[53] *TracePro User's Manul (Release 7.8)*.

[54] L. G. Henyey, J. L. Greenstein, *The Astrophysical Journal* **1941**, *93*, 70–83.

[55] I. J. Bigio, Sergio Fantini in *Quantitative Biomedical Optics (Theory, Methods, and Applications) 1st ed.*, Cambridge University Press, Cambridge, United Kingdom, **2016**, chapter 1, pp. 19–59.

[56] M. J. C. van Gemert, S. L. Jacques, H. J. C. M. Sterenborg, W. M. Star, *IEEE Transactions on Biomedical Engineering* **1989**, *36* (12), 1146–1154.

[57] L. Lin, Y. Chen, G. Li, J. Gao, K. Wu, in *Proceedings of SPIE 5630, Optics in Health Care and Biomedical Optics: Diagnostics and Treatment II*, (Eds: B Chance, M Chen, A. E. T. Chiou, Q Luo), SPIE, **2005**, pp. 486–497.

[58] D. Peng, H. Li, S. Xie, in *Proceedings of SPIE 6534, Fifth International Conference on Photonics and Imaging in Biology and Medicine*, (Eds: Q. Luo, L. V. Wang, V. V. Tuchin, M. Gu), SPIE, **2007**, pp. 1–6.

[59] D. Yudovsky, A. Nouvong, K. Schomacker, L. Pilon, in *Proceedings in SPIE 7555, Advanced Biomedical and Clinical Diagnostic Systems VIII*, (Eds: Tuan Vo-Dinh, Warren S. Grundfest, Anita Mahadevan-Jansen), SPIE, **2010**, pp. 755514 1–10.

[60] M. Sharma, R. Hennessy, M. K. Markey, J. W. Tunnell, *Biomedical Optics Express* **2014**, *5* (1), 40–53.

[61] L. O. Svaasand, L. T. Norvang, E. J. Fiskerstrand, E. K. S. Stopps, M. W. Berns, J. S. Nelson, *Lasers in Medical Science* **1995**, *10*, 55–65.

[62] I. V. Meglinski, S. J. Matcher, *Physiological Measurement* **2002**, *23*, 741–753.

[63] G. Altshuler, M. Smirnov, I. V. Yaroslavsky, *Journal of Physics D: Applied Physics* **2005**, *38*, 2732–2747.

[64] S. Wan, R. R. Anderson, J. A. Parrish, *Photochemistry and Photobiology* **1981**, *34* (4), 493–499.

[65] R. Marchesini, C. Clemente, E. Pignoli, M. Brambilla, *Journal of Photochemistry and Photobiology, B: Biology* **1992**, *16*, 127–140.

[66] R. C. Simpson, M. Kohl, M. Essenpreis, M. Cope, *Physics in Medicine and Biology* **1998**, *43*, 2465–2478.

[67] A. N. Bashkatov, E. A. Genina, V. I. Kochubey, V. V. Tuchin, *Journal of Physics D: Applied Physics* **2005**, *38*, 2543–2555.

[68] E. Salomatina, B. Jiang, J. Novak, A. N. Yaroslavsky, *Journal of Biomedical Optics* **2006**, *11* (6), 064026 1–9.

[69] C. Mignon, D. J. Tobin, M. Zeitouny, N. E. Uzunbajakava, *Biomedical Optics Express* **2018**, *9* (2), 852–872.

[70] Y. Wang, K. L. Marshall, Y. Baba, G. J. Gerling, E. A. Lumpkin, *PLoS ONE* **2013**, *8* (6), e67439 1–9.

[71] Y. Wang, K. L. Marshall, Y. Baba, E. A. Lumpkin, G. J. Gerling, *PLoS ONE* **2015**, *10* (3), 1–23.

[72] K. Chopra, D. Calva, M. Sosin, K. K. Tadisina, A. Banda, C. De La Cruz, M. R. Chaudhry, T. Legesse, C. B. Drachenberg, P. N. Manson, M. R. Christy, *Aesthetic Surgery Journal* **2015**, *35* (8), 1007–1013.

GRAPHICAL ABSTRACT FIGURE

GRAPHICAL ABSTRACT TEXT

Human skin equivalents (HSEs) are living cultures of skin tissue, grown by seeding fibroblasts and keratinocytes on a scaffold. Although devoid of chromophores, skin models are used to investigate the interactions between the epidermis and dermis, and

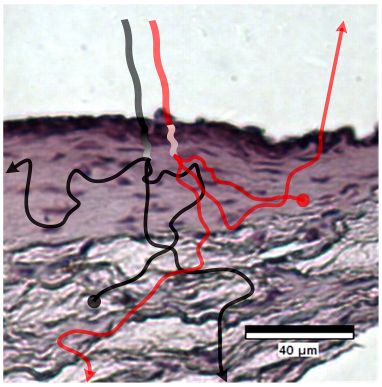

the morphology of skin layers. This article describes Monte Carlo simulations and experiments involving two-layer skin models. The measurements were comparable to the simulations, but only for samples thinner than 1 mm.

How to cite this article: A. Kallepalli, B. McCall, D. B. James, S. Junaid, J. Halls, and M. A. Richardson (2019), Optical investigation of three-dimensional human skin equivalents: A pilot study, *Journal of Biophotonics*

–